Size-frequency distribution of submarine mass movements on the Palomares continental slope (W Mediterranean)

Retegui, L.; Casas, D.; Casalbore, D.; Yenes, M.; Nespereira, J.; Estrada, F.; Canari, A.; Chiocci, F.L.; Idárraga-García, J.; Teixeira, M.; Ramos, J.; López-Gonzalez, N.

Published in:
Marine Geology

DOI (link to publication from Publisher):
10.1016/j.margeo.2024.107411

Publication date:
2024

Document Version
Publisher's PDF, also known as Version of record

Marine Geology 477 (2024) 107411

Contents lists available at ScienceDirect

Marine Geology

journal homepage: www.elsevier.com/locate/margo

Size-frequency distribution of submarine mass movements on the Palomares continental slope (W Mediterranean)

L. Retegui [a,b], D. Casas [c,*], D. Casalbore [d], M. Yenes [e], J. Nespereira [e], F. Estrada [c], A. Canari [c,f], F.L. Chiocci [d], J. Idárraga-García [g], M. Teixeira [h], J. Ramos [g], N. López-Gonzalez [i]

[a] Dpto. Ingeniería Cartográfica, Geodésica y Fotogrametría, Escuela Politécnica Superior, Universidad de Jaén, Campus Las Lagunillas s/n, 23071 Jaén, Spain
[b] Geodesy Group, Department of Sustainability and Planning, Aalborg University, Rendsburggade 14, 9000 Aalborg, Denmark
[c] Institut de Ciencies del Mar, CSIC, 08003 Barcelona, Spain
[d] Dip. di Scienze della Terra, Universita di Roma "Sapienza", 00185 Rome, Italy
[e] Dpto. de Geología, Universidad de Salamanca, 37008 Salamanca, Spain
[f] Faculty of Earth Sciences, University of Barcelona, UB, 08028 Barcelona, Spain
[g] Department of Physics and Geosciences, Universidad del Norte, Barranquilla, Colombia
[h] IDL (Laboratório Associado) – Instituto Dom Luíz, Faculdade de Ciências da Universidade de Lisboa, Edifício C1, Campo Grande, 1749-016 Lisboa, Portugal
[i] Instituto Español de Oceanografía-CSIC, Centro Oceanográfico de Málaga, Puerto Pesquero s/n, Málaga, Fuengirola 29640, Spain

ARTICLE INFO

Editor name: Michele Rebesco

Keywords:
Size–frequency
Mass movements
Inventory
Mediterranean
Power law

ABSTRACT

In this work, over 3620 km^2 from the Palomares continental slope, which is located in the W. Mediterranean Sea, was analysed to quantify the impact of recent mass movements on this margin. A total of 936 landslides were identified, mapped and characterised by defining several morphometric variables that outline the accumulated impact of landslides equivalent to 918 km^2 and 10.34 km^3 of eroded sediment on the continental slope. The smallest event area was 0.0014 km^2, whereas the largest event area was 32.48 km^2. Smaller scars with a higher headwall gradient tend to dominate when the environment is steeper, and major mass movements are located on open slopes and structural highs. However, the slight or null correlations between variables indicate that a wide range of sizes may occur on any slope gradient and at any depth.

The Palomares continental slope is intensively affected by mass movements. Compared with other passive margins (e.g., the U.S. Atlantic continental margin), landslides mobilised a limited amount of sediment, although it is comparable to other Mediterranean areas where small- to moderate-sized events are characteristic.

The cumulative size distribution can be defined by a power-law function that describes events larger than 0.7 km^2 with an exponent of $\alpha = 1.269$. These results are consistent with those of other published inventories, including onshore cases. This result allows us to assume that the scale-invariant properties of the events are mapped. Scale-invariant properties can be explained by different models; self-organised criticality (SOC) is probably the most assumed by the scientific community, although alternative models may be nominated. Each model has important implications in terms of the landslide distribution and long-term landslide history of any slope. Alternative scenarios, such as submarine slopes, with more precise landslide inventories may contribute to new hazard assessment models that consider scaling exponents derived from size–frequency distributions.

1. Introduction

Submarine slope instabilities are widespread processes that result in features collectively referred to as landslides, mass-transport deposits (MTDs), mass movements or instabilities. They involve diverse groups of complex sedimentary processes that are recognised as significant geomorphic processes on slopes (Densmore et al., 1998). Submarine slope instabilities are considered one of the main offshore geohazards since, through the effects of dragging, burial, undermining or direct impact, they can damage infrastructure, such as communication cables

* Corresponding author.
E-mail addresses: davidcasas@icm.csic.es (D. Casas), daniele.casalbore@uniroma1.it (D. Casalbore), myo@usal.es (M. Yenes), jnj@usal.es (J. Nespereira), festrada@icm.csic.es (F. Estrada), acanari@icm.csic.es (A. Canari), francesco.chiocci@uniroma1.it (F.L. Chiocci), idarragaj@uninorte.edu.co (J. Idárraga-García), macteixeira@ciencias.ulisboa.pt (M. Teixeira), jramosc@uninorte.edu.co (J. Ramos), nieves.lopez@ieo.csic.es (N. López-Gonzalez).

https://doi.org/10.1016/j.margeo.2024.107411
Received 29 December 2023; Received in revised form 23 September 2024; Accepted 5 October 2024
Available online 9 October 2024

or pipelines (Clare et al., 2017; Ercilla et al., 2021, among others). Landslide-generated tsunamis are also real threats to coastal communities (Clare et al., 2019; Ercilla et al., 2021; Harbitz et al., 2014).

Understanding submarine mass movements involves triggering factors (e.g., earthquakes), the nature of failed deposits and the prevailing conditions before failure, at failure and after failure. This approach requires geological and geomorphological data (e.g., classification and morphometry, distribution, sedimentary and morphosedimentary characteristics, and stratigraphy) and geotechnical data (e.g., strength and remoulded strength). All these variables, when available, are mostly used to characterise single slope failures rather than to provide a regional vision of the impact of these processes over a continental margin. (e.g., Kvalstad et al., 2005; Sultan et al., 2004).

Any realistic evolutive submarine-landscape model (e.g., the morphological evolution of slopes) should include long-term landslide rates. In this sense, regional inventories of mass movements (magnitude–frequency) and patterns in their distributions are essential (Galli et al., 2007; Guzzetti et al., 2012; Malamud et al., 2004). Often, the largest landslides are events of interest as case studies; however, even small landslides are important for obtaining a complete picture of the incidence of the process and for building a confident catalogue or inventory. This point is significant not only for achieving improved submarine landslide hazard analysis but also from a sedimentary point of view. The combined net sediment transport of small events may be as significant as that of individual large landslides (Casas et al., 2016; Clare et al., 2019).

The earth sciences are prolific for self-organised criticality (SOC) phenomena. The SOC was developed from a simple cellular automata model (Bak et al., 1988). It is linked to the framework of complex systems, which includes self-organisation (i.e., the process by which a natural system reproduces itself through its own elements and logic) and criticality, which refers to the evolution to a critical point where no lineal response is expected. Many interacting elements and their evolution towards a critical state, depending on minor changes in boundary conditions, define the SOC models. Formally, if a system exhibits an SOC, it evolves towards a critical state with scale-invariant properties where events of various sizes occur, and the distribution of event sizes follows a power law or tend towards a power law within the limit of infinite system size (Hergarten, 2002). Heavy rainfall, drainage networks or earthquakes follow a fractal (scale-invariant/power-law) size distribution, and there is evidence of mass movements (e.g., Guzzetti et al., 2012; Guzzetti et al., 2002; Hu et al., 2009; Micallef et al., 2008; Micallef et al., 2007; Turcotte, 1999). The scale-invariant properties of mass movements explained with an SOC model are quite recent and are sometimes assumed but are still under debate. This phenomenon is poorly understood (Hergarten, 2002; Tebbens, 2020). A cellular automaton or sandpile model is a simple model that likely cannot completely describe sedimentary instabilities; moreover, the number of observations in which the distribution appears to be a power law is low compared with that of earthquake statistics, which are documented by extensive records and catalogues (Guthrie and Evans, 2004; Guzzetti et al., 2002; Malamud et al., 2004). This fact emphasises the urgency of increasing the modelling of mass movement statistics.

For any landslide hazard assessment, a deterministic analysis is needed. However, understanding whether the long-term evolution of landslide activity is explained by progress towards the critical state could help us understand the temporal distribution of, in particular, large mass movements. In the critical state, large events are less likely than small events (Hergarten, 2002). No slope stability models account for the scale-invariant properties of mass movements; thus, there could be a potential research area where scaling is part of the probabilistic landslide hazard assessment (Guzzetti et al., 2005).

The objective of this work is to explore the morphometry, size distribution and potential scale-invariant properties of 936 submarine landslides mapped within the southern Iberian continental margin, Palomares, where mass movements are extensively spread throughout the continental slope (Fig. 1). The aim of this study is also to contribute to increasing regional mass movement inventories in marine environments where data remains poor because of the limited availability of high-resolution data and to contribute to the global data available for mass movement statistics.

2. Geological setting

The Palomares continental margin, located in the Iberian Peninsula Gulf of Vera (SW Mediterranean Sea), evolved between the eastern internal zones of the Betic Cordillera and the Algerian basin (Fig. 1). The study area is located in a scenario of continuous NW–SE convergence between the Eurasian and African plates, generating the Aguilas Arc tectonic indentation structure and southeastward tectonic tilting of the margin (Coppier et al., 1989; Fig. 1).

Several tectonic and sedimentary features shape the continental margin, including structural highs (Aguilas, Abubacer and Maimonides); submarine canyons (Gata, Almanzora-Alias-Garrucha and Aguilas); sedimentary systems, such as contourites and mass movements; and salt diapir intrusions on the distal margin and Algerian abyssal plain (Ercilla et al., 2022; Gómez de la Peña et al., 2016; Fig. 1).

The seismic stratigraphy features an irregular basement, is metamorphic and volcanic in origin, and is covered by upper Miocene and Plio-Quaternary sediments (Ercilla et al., 2022; Giaconia et al., 2012; Gómez de la Peña et al., 2016). The basement was subaerially exposed during the Messinian salinity crisis produced by Mediterranean Sea isolation (Estrada et al., 2011). Plio-Quaternary sedimentation was defined by bottom currents and contourites after the restoration of marine conditions (Alonso et al., 2023; Ercilla et al., 2016; Juan et al., 2020; Juan et al., 2016). Mass movements have been described throughout the whole margin, affecting mainly continental slope contourite deposits.

The present-day continental slope is defined as a narrow and steep upper slope, a smooth and gentler platform and a lower slope with highly irregular gradients (Fig. 1). The intraslope Gata Basin has been identified between the slope platform and the Abubacer High (Ercilla et al., 2022).

3. Data and methods

The Palomares continental margin was surveyed with swath multibeam systems several times for different purposes and at different institutions. This study merged 2 sets of data obtained with 2 deep-sea multibeam echosounders, the KS EM12 (13 kHz) and the Atlas Hydrosweep DS (14–16 kHz). The first set resulted in a 50 m resolution digital elevation model (DEM), which covers the southern part of the study area (Fig. 2) and was provided by the General Spanish Secretary for Fisheries (SGP). The second dataset was acquired in the framework of the FAUCES project (Casas et al., 2019), allowing the generation of a 15 m resolution DEM that covers the area of the Garrucha canyon and its margins (Fig. 2). Furthermore, the FAUCES project provided TOPAS (topographic parametric sonar) profiles. TOPAS is a very high-resolution seismic tool with penetration <150 m and resolution up to cm. The tool uses the nonlinear propagation of waves through water to generate a low-frequency acoustic pulse from intermodulation high-frequency pulses. The system operates with a primary frequency of 18–39 kHz and a secondary frequency between 0.5 and 6.0 kHz.

The methodological approach for the inventory does not rely on the study of a specific landslide but rather relies on the complete mapping of all the events present in the study area. In this sense, the terms submarine mass movements, instability or landslides are used in this work synonymously, and include all types of sedimentary instability processes without distinction.

The inventory of instabilities is attained by identifying landslide failure scars and headwall domains given that the absence of a uniform and dense seismic profile grid prevents the correct definition of deposits

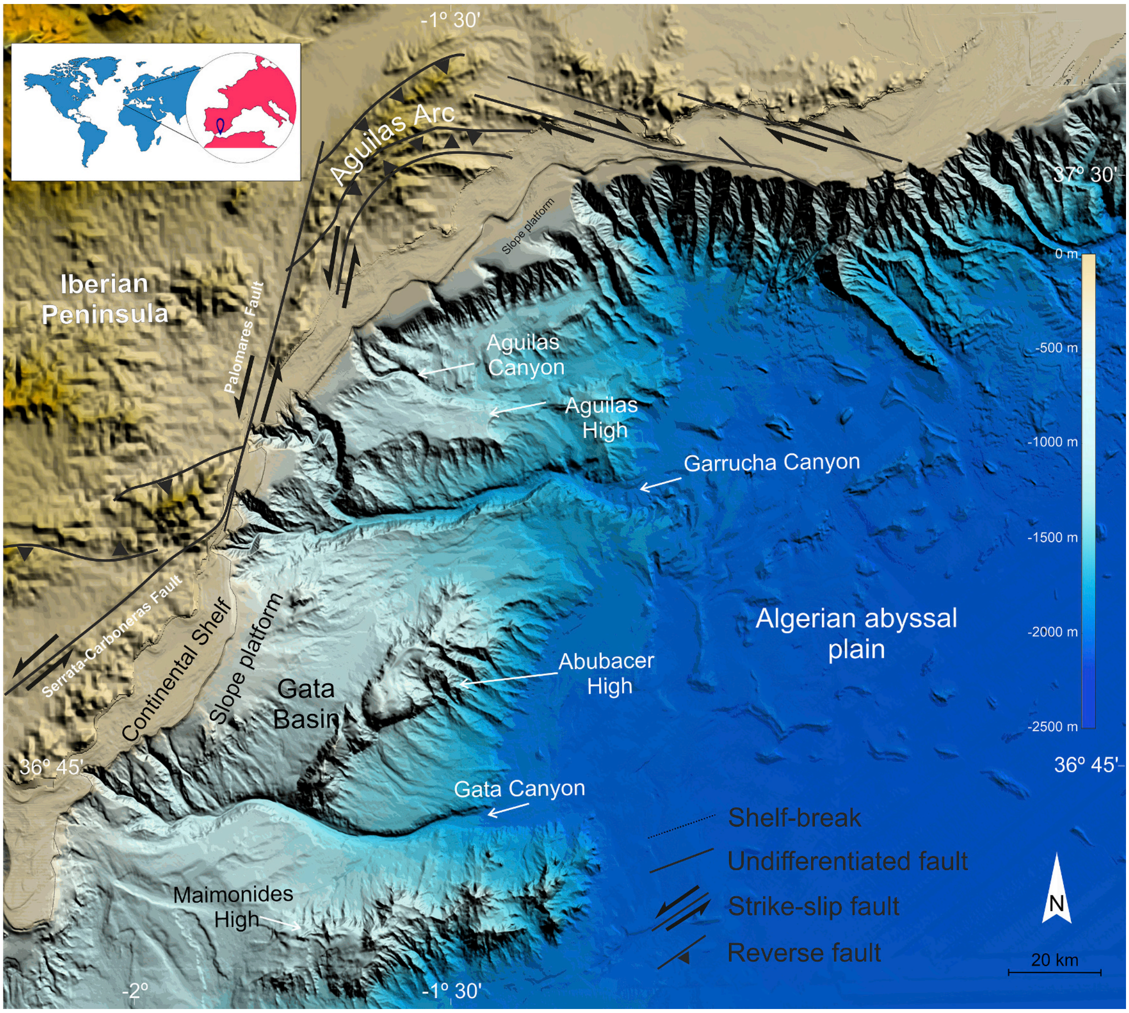

Fig. 1. Physiography and main features defining the Palomares continental margin located in the Iberian Peninsula Gulf of Vera (SW Mediterranean Sea). Several tectonic and sedimentary features shape the continental margin, including structural highs (Aguilas, Abubacer and Maimonides), submarine canyons (Gata, Garrucha and Aguilas), and sedimentary systems, such as contourites and mass movements. The Garrucha canyon is formally the Almanzora-Alias-Garrucha canyon.

(e.g., length or thickness of 936 events over the 3620 km^2 analysed). Among all possible procedures (e.g., ten Brink et al., 2006; Völker et al., 2011; Clare et al., 2019), the area and volume of sediment displaced by each event were calculated following the methods described by Chaytor et al., 2009 or Casas et al., 2016. The morphology observed in the bathymetry does not offer a coherent solution in defining the area affected by deposits associated with each event; this is especially true when events have different ages and the displaced sediment has been reworked and transported in different ways, generating diffuse or invisible footprints in most cases. Therefore, the definition of the evacuation/erosive zone has been found to be a viable alternative for approaching the size of each event. This area should be bounded by the scars (headwalls and sidewalls) of each event (Fig. 2). Defining the limit between evacuation areas and deposits is an exercise with a high degree of interpretability and may produce inconsistencies. The degree of inaccuracy is a good geomorphological tool because it is centred on the easy identification of a prominent morphological feature compared with the mass movement boundaries, and at the same time allows the quantification of the minimum amount of sediment involved in each event. The method applied is therefore defined by the identification and cartography of landslide scars and, subsequently, the digitalisation of the bounding polygon that encompasses the region of negative elevation within the headwall and sidewalls corresponding to the sediment evacuation area (Fig. 2). The scars and areas were identified by examining DEMs with different illuminations and slope maps/slope profiles.

The volume of sediment involved (displaced) for each observed event was approached by the empirical relationship between the headwall area (A) and volume (V) in the form of $V = 0.009A^{1.3689}$. This relationship was established by calculating the volume between the surface defining the evacuation area and the synthetic surface simulating the presliding slope for more than 400 events in the Tyrrhenian Sea (Casas et al., 2016).

For each event, different morphometric parameters were retrieved: the surface of the eroded area, the depth of the scar, the gradient and height of the headwall, the length and sinuosity of the scar and the gradient of the surrounding slope. All these parameters may contribute to improving the use of other existing databases in marine environments (León et al., 2020; León et al., 2018; Urgeles et al., 2023).

The identified scars, i.e., only those with surficial expressions, were classified as recent or subrecent instability events not associated with the timing or type of instability. Juxtaposed seafloor scars, e.g., small scars found to overlap with larger scars, have been identified as independent features to avoid the overestimation of large events.

3.1. Size–frequency

Magnitude–frequency distributions (e.g., noncumulative and cumulative frequency, probability density or frequency density distributions) are critical for understanding natural hazards, such as mass movements. Instabilities seem to have magnitude–frequency distributions that follow

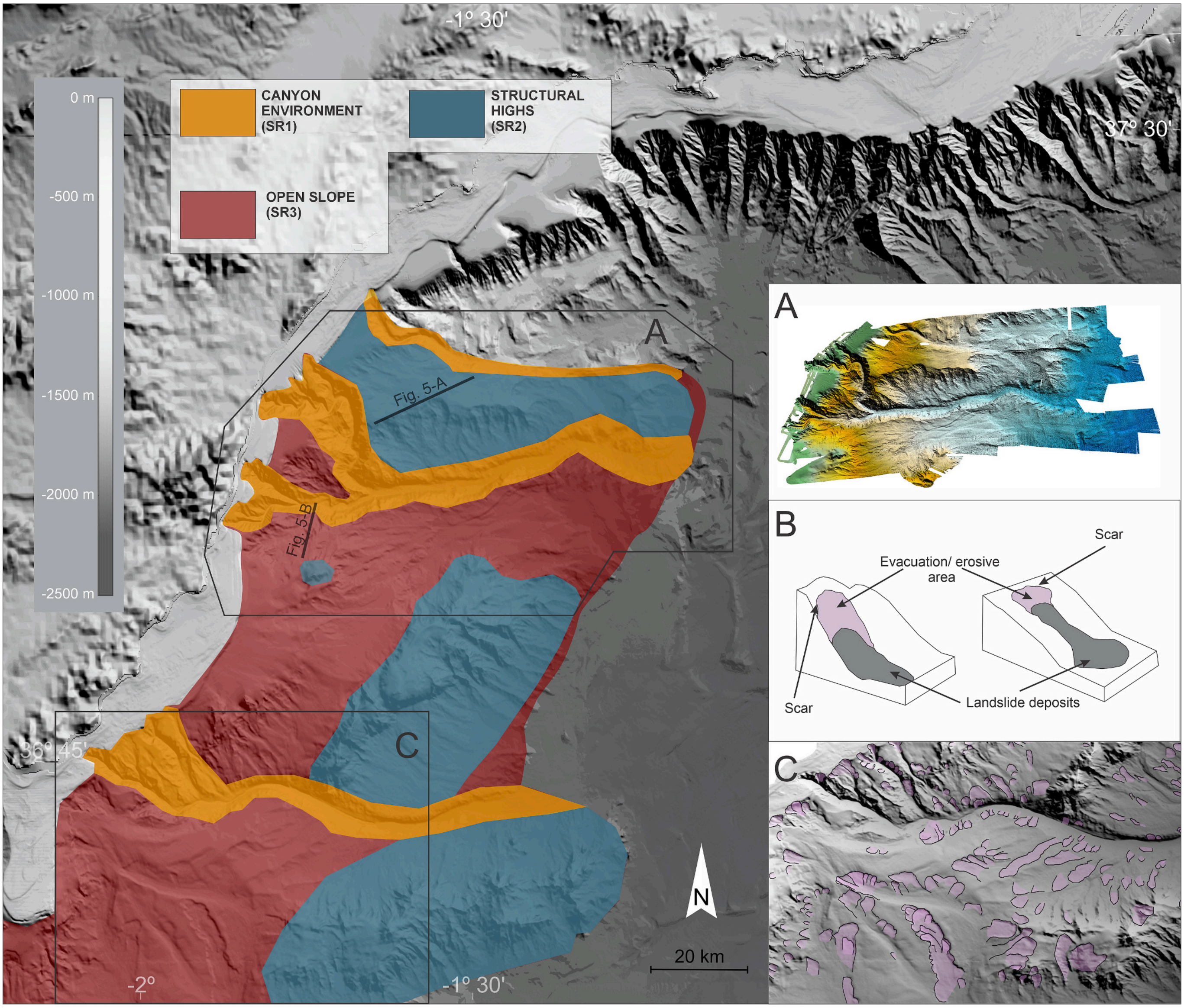

Fig. 2. Map of the areas corresponding to subsets SR1, canyons and channels; SR2, structural highs and ridges; and SR3, open slope. Topas profiles that appear in Fig. 5 are located. The study merged 2 DEMs, the first with a 50 m resolution, which covers the southern part of the study area, and the second with a 15 m resolution, which covers the area of the Garrucha canyon and its margins (upper box A). The definition of the evacuation/erosive zone has been found to be a viable alternative for approaching the size of each event. This area should be bounded by the scars (headwall and sidewalls) of each event (box B). Details of the study area where scars and areas (in purple) can be observed in box C. (For interpretation of the references to colour in this figure legend, the reader is referred to the web version of this article.)

power-law functions for both area and volume, although other functions (e.g., log-normal, logarithmic, etc.) have been tested (Chaytor et al., 2009; Haflidason et al., 2005; Puga-Bernabéu et al., 2022; ten Brink et al., 2006; Urgeles and Camerlenghi, 2013). Because one of the aims of this work was to test the scale-invariant properties of the events described, in-depth discussion about which function fits better is not provided. Only heavy-tailed distributions, such as power laws, have been tested for analysing the scale-invariant properties of sizes. To determine this value, the plot of the cumulative size distribution (i.e., the probability function) on logarithmically scaled axes must be approximated to a straight line (Hergarten, 2002). Regardless of whether the obtained cumulative size distribution exhibits a clean power law behaviour over a reasonable range, a scale-invariant distribution may be assumed. In this case, the scaling exponent corresponds to the slope of the straight line (Hergarten, 2002). The power–law functions were fitted via linear regression via the least squares method, and plots were generated from MATLAB software.

4. Results

4.1. Mass movements in the Palomares continental margin

Within the 3620 km^2 analysed, 936 scars were identified (Figs. 2 & 3). Instabilities are widely distributed; therefore, to better clarify the distribution of instabilities, the study area was divided into three environmental areas or subregions (SRs): SR1, canyons and channels; SR2, structural highs and ridges; and SR3, open slope (Figs. 2& 4).

When topographic parametric sounder (TOPAS) profiles are available, the instabilities are characterised by irregular to lens-shaped or wedge-shaped transparent acoustic facies (Fig. 5); they rest both on the seafloor surface and buried below it, forming stacked deposits, or they are found interbedded within other sediments, such as contourites and

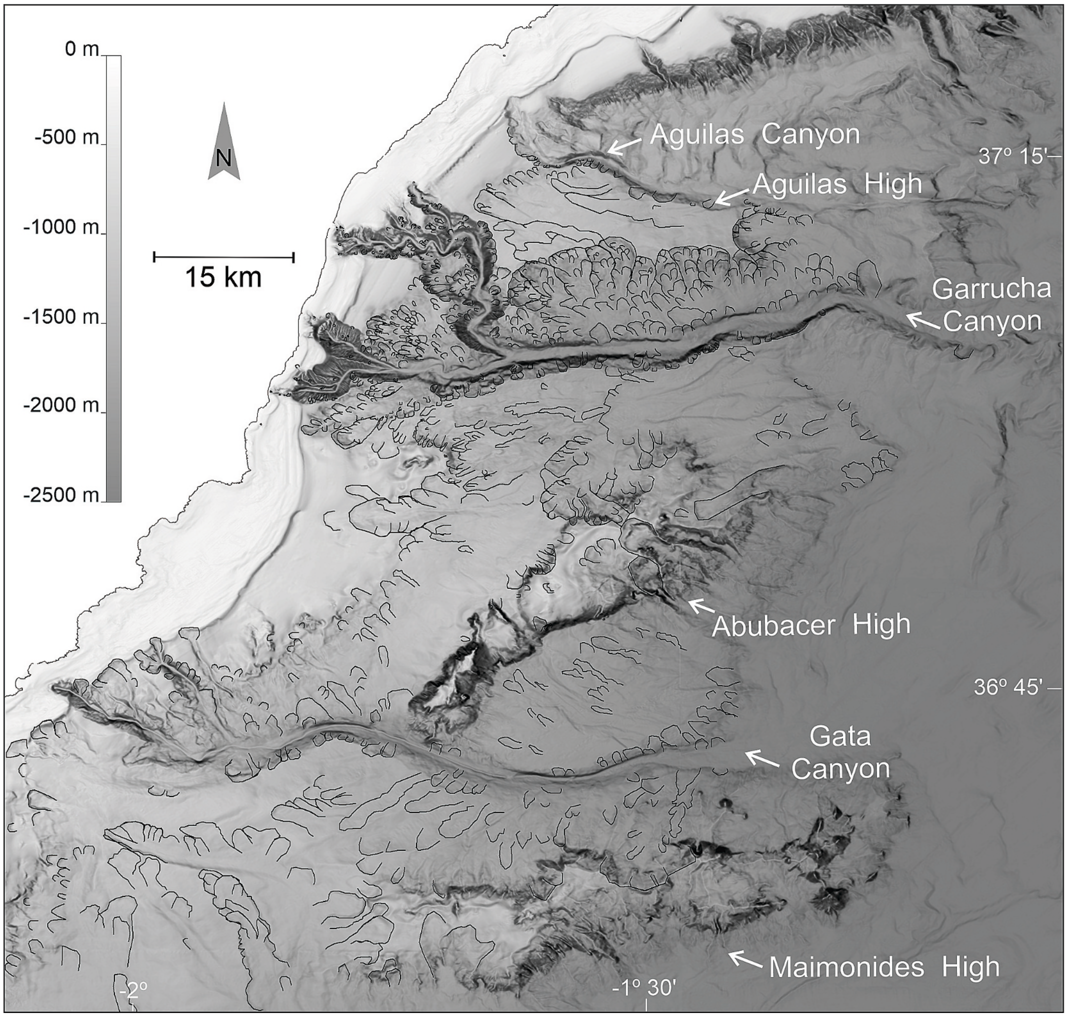

Fig. 3. Shaded relief map of the study area (3620 km^2) and the 936 scars inventoried. The smallest landslide identified (0.0014 km^2) was defined by a 124.1 m long scar at a water depth of 68 m (mwd), and the largest landslide (32.48 km^2) by a scar of 36.61 km at 1036 mwd.

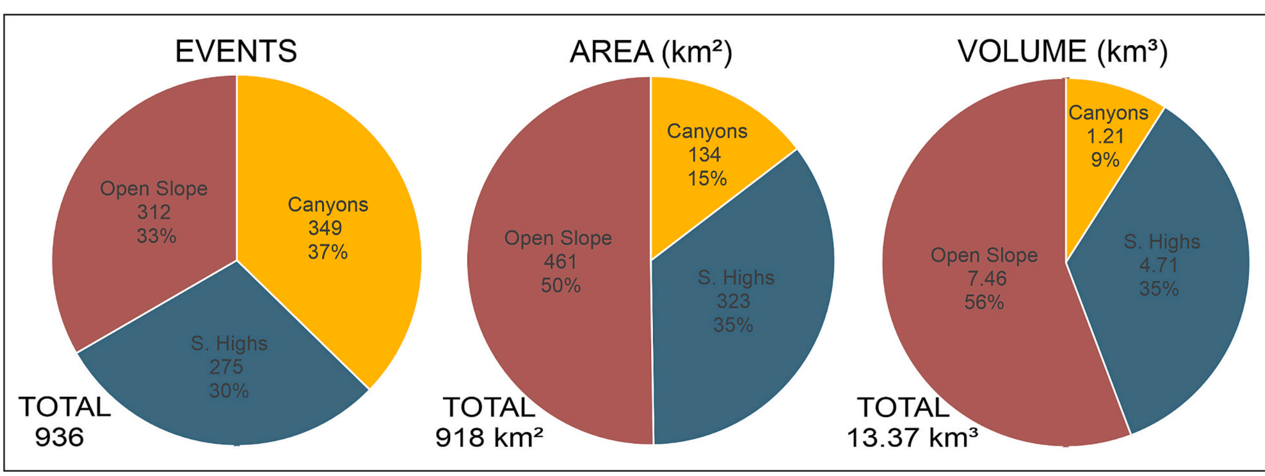

Fig. 4. Total observations of scars and related headwall areas. Instabilities are quite balanced between SR1, canyons and channels; SR2, structural highs and ridges; and SR3, open slopes. The largest instabilities are located in SR3 (with a total affected area of 461 km^2), whereas SR1 has the maximum number of small events, affecting a total area of only 134 km^2 but a volume of only 1.2 km^3.

hemipelagites (Ercilla et al., 2022).

These instabilities affected a cumulative area of 918 km^2 (Fig. 4). The mean area of the events was 0.85 km^2, and the smallest and largest areas were 0.0014 km^2 and 32.48 km^2, respectively (Table 1). The largest event was located at a 1036 m water depth (mwd) and was associated with a 36.61 km long scar. The smallest scar was located at 68 mwd and

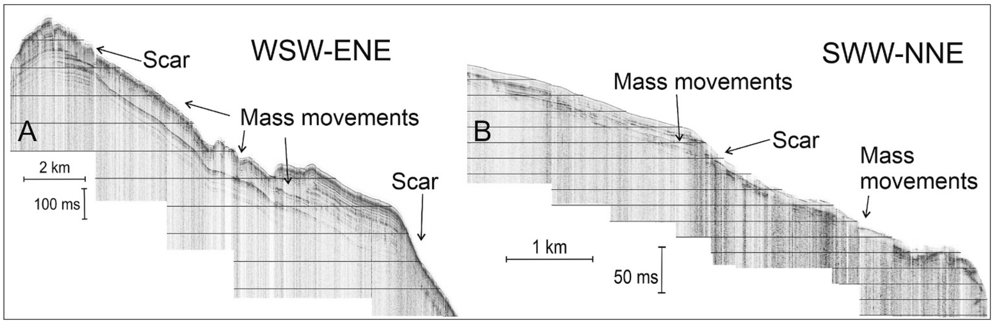

Fig. 5. Topas profiles with examples of mass movements and scars affecting highs (A) and canyon heads (B). Instabilities are both on the seafloor surface and buried below it, forming stacked deposits, or they are found interbedded within other sediments, such as contourites. Only seafloor surface features were included in this study. The profiles are shown in Fig. 2.

Table 1
Summary of the main morphometric parameters of instabilities mapped along the Palomares continental margin.

	Average	Min	Max
Scar length (km)	2.60	0.12	36.61
Perimeter (km)	3.25	0.14	38.50
Area (km^2)	0.85	0.0014	32.48
Headwall height (m)	52.84	2.10	327.20
Headwall gradient (°)	14.71	1.70	49.70
Regional gradient (°)	9.95	0.60	35.00
Scar minimum depth (m)	−1100.34	−27.92	−2370.63
Scar maximum depth (m)	−1221.30	−61.08	−2418.83
Scar sinuosity	4.56	1.20	19.48

Table 2
Summary of the main morphometric parameters characterising the instabilities mapped in SR1, canyons and channels; SR2, structural highs and ridges; and SR3, open slope.

Averages	Canyons	S. Highs	Open slope
Scar length (km)	1.58	3.03	3.43
Perimeter (km)	2.08	3.86	4.39
Area (km^2)	0.38	1.17	1.48
Headwall height (m)	60.78	60.28	42.15
Headwall gradient (°)	22.70	8.73	11.66
Regional gradient (°)	14.16	10.74	6.46
Scar minimum depth (m)	−980.49	−1410.52	−956.67
Scar maximum depth (m)	−1116.42	−1550.52	−1070.42
Scar sinuosity	4.68	4.09	4.48

is bounded by a 124.1 m long scar.

The distribution of the total number of identified events among the three subregions was quite balanced (Fig. 4). SR3 (open slope) has the largest instabilities, with a total affected area of 461 km^2, whereas SR1 (canyons and channels) has the maximum number of events but also has the smallest instabilities, affecting only 134 km^2 (Fig. 4).

The empirical relationship between the headwall area (A) and volume (V) selected in this work ($V = 0.009A^{1.3689}$; Casas et al., 2016) is justified by the similarity, from a sedimentary and geomorphological point of view, with the area where it was defined. The area–volume relationships reported in different regions of the world (in subaerial and submarine environments and for soil/sediment) show exponential values ranging from 1.09 to 1.45, which are likely related to different instability processes (Chaytor et al., 2009; Guzzetti et al., 2009; Klar et al., 2011; Moscardelli and Wood, 2016).

The calculated volumes of sediments involved in mass movements can help to determine the extent of erosion in the area, and for this study, this case was equivalent to a total volume of 13.37 km^3 of displaced sediments (Fig. 4). The calculated volumes ranged between 1099 m^3 (1.099 E-6 km^3) and 1.05 km^3, with a mean value of 0.014 km^3.

4.2. Morphometry

The morphometric parameters measured for the scar features included in the inventory are summarised alongside their value ranges in Table 1. The values of those parameters for scars grouped in the defined subregions are detailed in Table 2.

The identified instabilities exhibit scar lengths and perimeters ranging between 0.1 km and 36 km long, with areas ranging from 0.001 km^2 to 32.48 km^2 and a mean value of 0.85 km^2. The headwall heights vary between 2.1 m and 327.2 m, whereas the headwall gradients range between 1.7° and 49.7°. Moreover, the identified scars are located in areas with regional gradients of 0.6°–35.0° and water depths ranging from 27.9 m to approximately 2420 m. The sinuosity indices of the scars range between 1.2 and 19.5.

Pearson correlation coefficients were computed between the measured variables detailed in Tables 1 and 2, with the aim of verifying whether correlations existed. Very low correlations (i.e., <0.5) between most of the variables were found (supp. material). The scar length and headwall area had a good correlation (0.88), and the headwall gradient and slope gradient had a slight positive correlation coefficient of 0.52. The slope gradient, in turn, was negatively correlated with the scar perimeter (−0.39) and scar length (−0.35).

4.3. Magnitude–frequency distribution

The noncumulative distribution clearly shows that small events (< 1 km^2) are more frequent in SR1 (canyons), whereas the largest scar areas in the inventory (>1 km^2) are more frequent along the open slope (Fig. 6; Table 2). The adjustment to a log-normal distribution reveals a characteristic size of 0.356 km^2 for the whole margin (the area to which the logarithmic mean corresponds; Fig. 7). This size is greater for SR3 (open slope), with a value of 0.578 km^2, whereas it reaches the lowest value for SR1 (canyons), with a value of 0.160 km^2 (Fig. 7).

The cumulative size distribution (probability function) allows us to test the potential scale invariance properties of the dataset. The power-law distribution was tested for the whole dataset as well as for every subregion (Fig. 8). For all the data and subdatasets, the headwall area partially fits an inverse power law from a cut-off threshold (where the distribution is below the power function). At sizes less than the cut-off point, 0.7 km^2 are underrepresented by the power law function that describes the largest events with an exponent of $\alpha = 1.269$. For all the subregions and data with different resolutions, the power law is valid for similar orders of magnitude, with exponents α in the range of 1.1–1.49. (Table 3; Fig. 8). Therefore, these results seem to be consistent with the scale-invariant properties of the studied dataset.

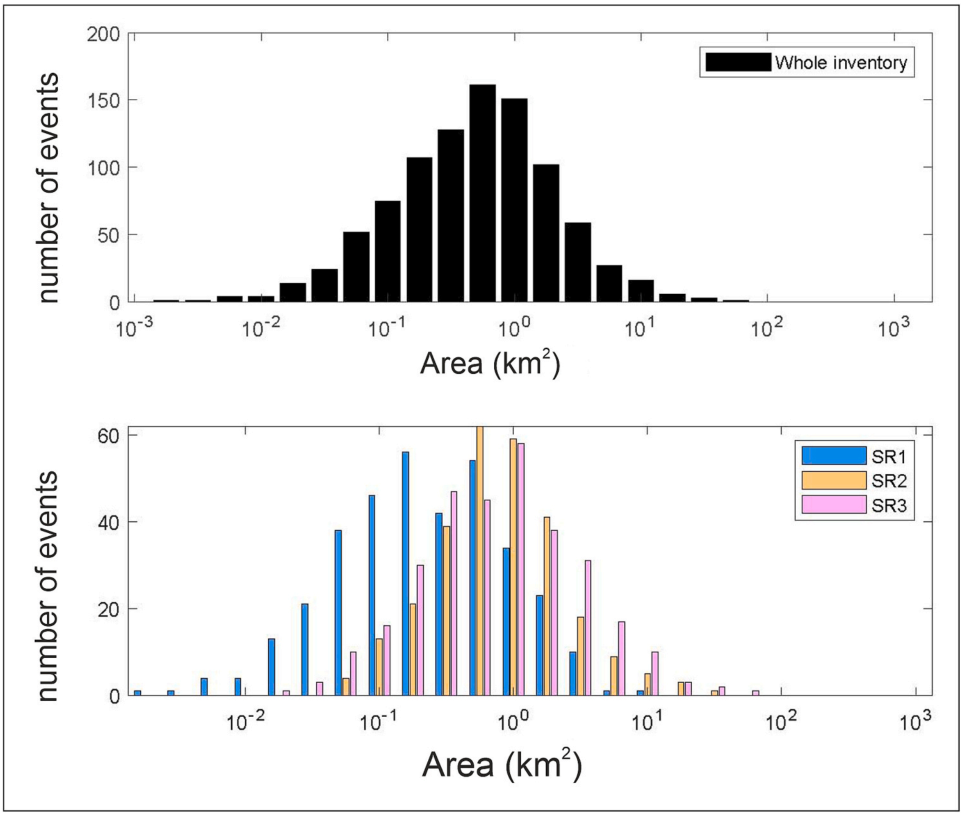

Fig. 6. Frequency/area of the headwalls for the Palomares margin. The largest scar areas in the inventory (>1 km^2) are more frequent along SR3.

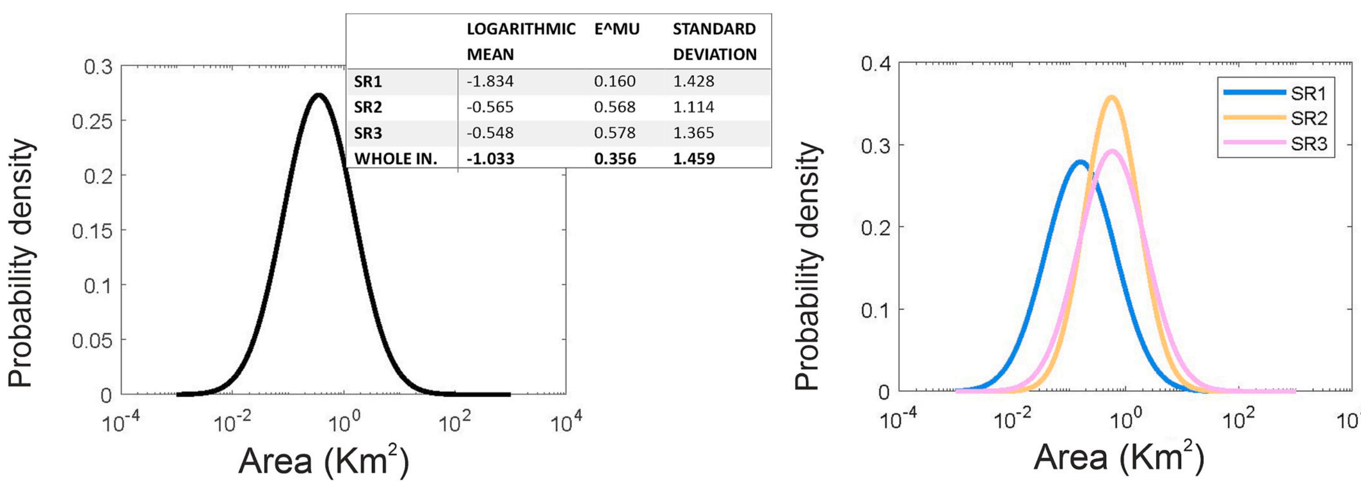

	LOGARITHMIC MEAN	E^MU	STANDARD DEVIATION
SR1	-1.834	0.160	1.428
SR2	-0.565	0.568	1.114
SR3	-0.548	0.578	1.365
WHOLE IN.	**-1.033**	**0.356**	**1.459**

Fig. 7. Density function for the whole inventory and subsets, fitted to a lognormal function. The results of the density functions allow us to define the characteristic size in the study area (0.356 km^2), while it is 0.160 km^2 for SR1 and 0.57 km^2 and 0.58 km^2 for SR2 and SR3, respectively. The table shows the area to which the logarithmic mean corresponds. (E^mu) and the standard deviation (STD).

5. Discussion

5.1. Morphometry and subregions

The scarce slight significant correlations found between most morphometric variables, e.g., headwall gradient/slope gradient or slope gradient/scar perimeter/scar length, may indicate that the geometry of the environment might exert some, but limited, control over the dimension of events, enhancing smaller scars with a higher headwall gradient when the environment is steeper. However, although the slope gradient is important for slope stability, the topographic slope alone does not sufficiently explain the size distribution on almost any slope (ten Brink et al., 2006). Notably, large submarine instabilities can occur on 1–2° slopes, while such gradients may be considered stable on land (Hühnerbach and Masson, 2004; Urlaub et al., 2013). Even so, from the correlations obtained, a wide range of sizes may occur on any slope because there is no characteristic size for a particular slope gradient or slope size; there are only tendencies; this means that stability depends on a variety of factors in addition to the slope gradient and other components related to the mechanical properties of sediments, such as those related to the pore pressure, which may change over time.

The observed landslides are almost equally distributed among the

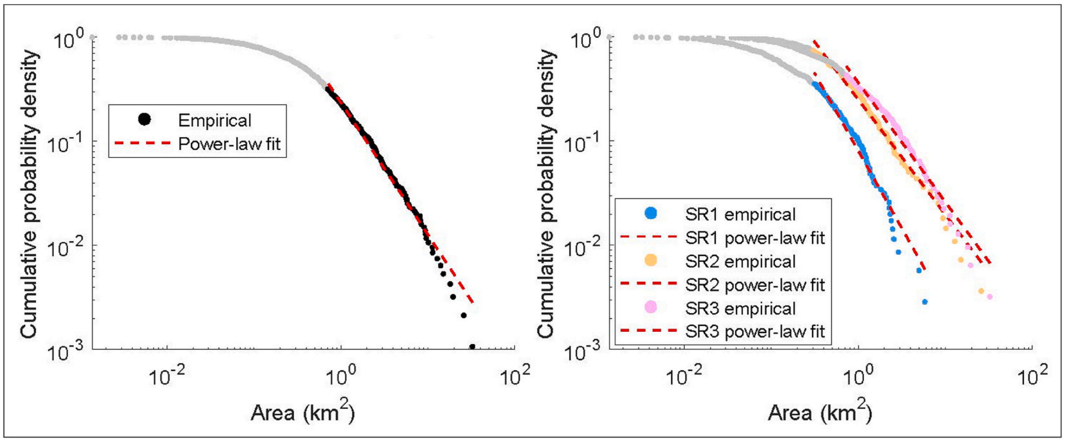

Fig. 8. Plots of the cumulative probability density of the area for the whole inventory and for each subregion. The inverse power law model fits very well when describing events larger than 0.7 km^2.

Table 3
Inverse power law parameters. At sizes larger than the cut-off point, 0.7 km^2, the power law function has an exponent of $\alpha = 1.269$. For all the subregions, the power law is valid for similar orders of magnitude, with exponents α in the range of 1.1–1.49.

	Exponent	Validity range	R^2
SR1	1.486	0.3–5.8	0.968
SR2	1.104	0.3–25.91	0.984
SR3	1.146	0.7–32.48	0.971
Whole in.	**1.269**	0.7–32.48	**0.987**

three analysed subregions. Those associated with the canyon environment (SR1) represent 37 % of the total inventory but are also smaller, accounting for only 9 % of the mobilised sediment volume (Fig. 4). In the canyon walls, high slope gradients are found (14° on average), which is the maximum contribution to the slight negative correlation found between regional gradients and scar length (−0.35) at the regional level. Different works show an inverse relationship between the slope angle and pore water pressure because a higher flux of water and percolation develop with increasing slope, allowing lower pore water pressures within seabed sediments (Rafiei et al., 2019; Wang et al., 2023). In this context, erosion and the local effect of oversteepening should play a preferential role as triggers on the canyon walls studied where small events dominate.

One highly positive correlation, which was valid for the 935 events observed, was between scar length and headwall area or evacuation area (0.88). In general, the area, volume and thickness of mass movements are strongly correlated; therefore, the conversion of these variables is a good approach for determining their distribution (e.g., Hovius et al., 1997; Pelletier et al., 1997). Measurements of area tends to be more reliable than measurements of volume; however, such measurements could also be difficult when events have diffuse or invisible bathymetric footprints. In contrast, scars are prominent features that are easily discernible in bathymetric maps. For those cases, the size of events can be approached with the relationship between scar length and area (Fig. 9):

$$\text{Area} = 0.1188^{*}\text{length}^{1.7424}$$

This approach is regional and must be contrasted across different areas, geological contexts or types of instabilities.

The smallest and largest sizes mapped are 0.0014 km^2 (at 68 mwd) and 32.48 km^2 (at 1036 mwd), respectively. According to the observations summarised in Fig. 4, the ten major events mapped (i.e., > 10 km^2) are distributed between SR3 (6 events) and SR2 (4 events) and between 870 and 1992 mwd. The ten minor events mapped (<0.0095 km^2) are all

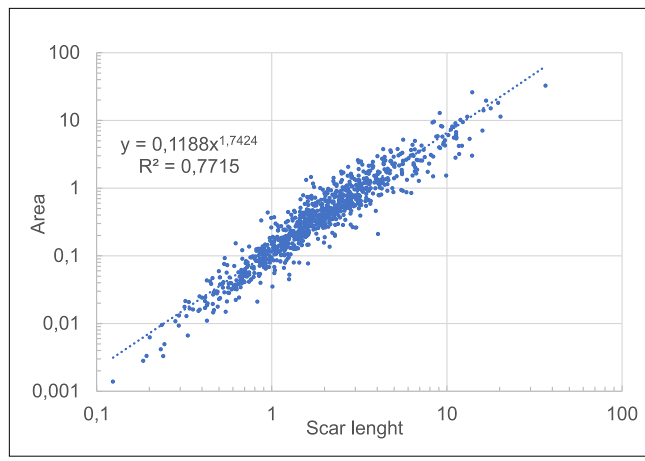

Fig. 9. Scars are prominent features easily discernible in bathymetric maps. For those cases where the measurement of area is difficult with only bathymetric data, the size of events can be approached, for the study area, with the relationship obtained with the whole inventory, between scar length and area.

located on SR1 between 51 and 765 mwd; this means that mainly open slopes and structural highs cluster the major mass movements, whereas canyons are affected by minor events. Despite this fact, the practically negligible correlation between depth and size (−0.15/−0.06; Supplementary material) means that no relevant pattern is considered for hazard assessment. A wide range of sizes can occur at any observable depth.

5.2. Scale-invariant properties

Different studies have shown evidence of scale-invariant characteristics of mass movements, resulting in a heavy-tailed distribution; this means that large events follow a power law given that most datasets obtained from nature do not exhibit characteristic behaviour at small sizes (Clauset et al., 2009). Different works attribute this effect to factors such as undersampling (Guthrie and Evans, 2004; Tanyaş et al., 2019), changes in the physics of large/small-scale mass movements (Stark and Guzzetti, 2009), geomorphology (Guthrie and Evans, 2004), and even sampling resolution differences due to temporal sampling factors (Williams et al., 2018). The statistical approach used to test scale invariance or scale-dependent distributions may considerably affect or lead to biased results (Tebbens, 2020). The discussion of which is the best method is outside the scope of this work. However, in general, if the cumulative size distribution follows a clean power law, a scale-invariant distribution can be assumed, and the slope in the logarithmic plot is the scaling exponent (Hergarten, 2002). The uncertainty in determining the exponents is obvious when bibliographic results are compiled and compared with the results of this study (Table 3). Mostly from onshore inventories and using cumulative and noncumulative frequencies, as well as density distributions covering different ranges, systematic variations in scaling exponents are reported: 1.16 (Hovius et al., 1997); 1.46 and 1.11 (Stark and Hovius, 2001); 0.96 (Fuyii, 1969); 1 (Sugai et al., 1995); 1.6–2 (Pelletier et al., 1997); 1.4–3.5 (Van Den Eeckhaut et al., 2007); and 1.8–3.3 (Tanyaş et al., 2019). Other recent marine inventories yielded exponents of 1.5–1.7 (Casas et al., 2016) and 1.49 (Puga-Bernabéu et al., 2022) in different geologic frameworks.

In addition to the model, which can explain fractal statistics in mass movements, accurate determination of landslide scaling is important for describing the relative contributions of large/small events and for quantifying and comparing different landslide inventories and validation models (Fig. 10). This is evidenced when the two different bathymetric resolutions used in this study, medium- and high-resolution datasets, are studied individually. Smaller events are detected at a higher resolution, which could bias the results. To test this hypothesis, the cumulative size distributions for both subsets were calculated, and although the cut-off points were slightly different, the scaling exponents were similar (Fig. 10). We can assume that the large/small size ratio is not significantly affected. Although the use of homogenous and as-high-as-possible resolution has to be the main target of a new inventory, in this particular case, the impact seems not to be significant, and the result is not distorted.

5.3. Critical landscapes

A model that may explain scale invariance is self-organised criticality (SOC), which is based on a cellular automata model that frames dynamic systems evolving by local interactions (Bak et al., 1988; Evesque, 1991; Nagel, 1992). SOC has interesting implications from a geomorphological point of view in terms of landscape evolution and hazard assessment.

First, it implies the universality of the scaling exponent, i.e., a fixed ratio of small/large number of landslides (Hergarten, 2002). Rigorous statistical tests over new and extensive observations, including those located in marine environments, are critical to determine the variability of scaling exponents observed.

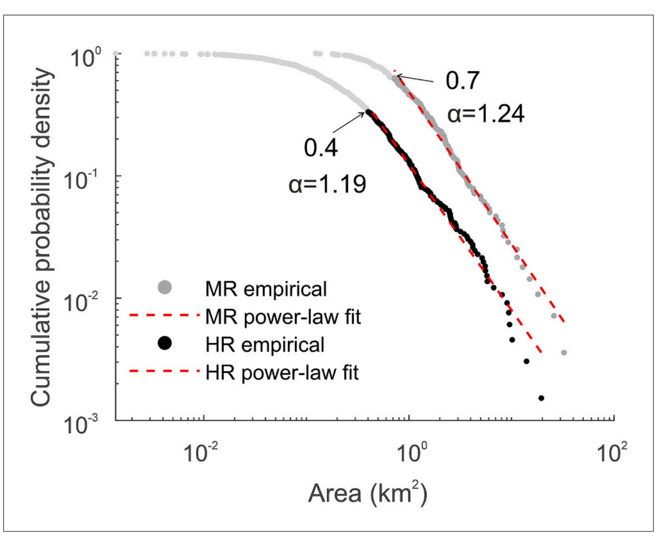

Fig. 10. Plots of the cumulative area for two subsets: high-resolution (HR) and mid-resolution (MR) images. The scaling exponents are practically equivalent (1.2), whereas the cut-off point decreases from 0.7 km^2 to 0.4 km^2 for the high-resolution subset.

Second, following the cellular automata model and power law distribution, a landslide propagates from nucleating sources in avalanche form (Bak et al., 1988; Micallef et al., 2007). Most likely, this model cannot represent the complexity of the dynamics of sedimentary instabilities. The diversity of processes and transformations pre- and postfailure involved in each possible event is a product of the physical and geotechnical properties of the mobilised sediment (sorting, porosity and permeability, mineralogy and grain size, etc.) but also of processes such as hydroplaning, which favours long runouts and low erosion of mobilised sediment (Hampton et al., 1996; Hungr et al., 2014; Locat and Lee, 2002; Mulder and Cochonat, 1996; Shanmugam, 2019).

Some kinds of grain flow may be comparable to Back's sandpile avalanche model, and at least qualitatively, creep (i.e., slow, long-term sediment deformation under a constant load) (Nardin et al., 1979) could be similar to avalanche propagation in SOC models. In this model, instability is triggered in a small part, and the load is transferred to the vicinity, where it spreads over a larger area of undetermined size. Creep can be considered a precursor of instability, and propagation depends on the spatial distribution of driving forces and shear strength along the slope, which is the result of the geological history of the slope and is therefore dominated by long-term factors controlling stability. The SOC model can be used to understand the complex evolution of slopes as a system evolves towards a state with an explicit statistical distribution and spatial correlations. In addition to field measurements (mostly on land), different stochastic models can generate synthetic inventories of mass movements where the size distribution shows power-law behaviour (Densmore et al., 1998); however, additional field observations are needed, and additional research on the evolution towards and meaning of the critical state for landscapes and mass movements is needed, accounting for all the potential physical transformations involved in mass movement processes. The open question related to the time dependency of the model (long-term factors), the time required to reach a power-law distribution or the tuning of the system to changing geological conditions (sea level, tectonics, etc.) also requires new data, such as confidence in the timing of the observed triggering mass movements.

As an alternative to the SOC model, the scale-invariant properties of mass movements could be linked to the fractal properties of triggers such as earthquakes or, if we consider terrestrial environments, heavy rainfall (e.g., Feder, 1988; Turcotte, 1999). However, there is empirical evidence that a single earthquake may trigger many landslides with a size distribution similar to that of long-term observations (Harp and Jibson, 1995). Pelletier et al. (1997) also reported that there are no differences between rainfall and earthquake-triggered mass movements. Non-SOC models based on variables such as soil property distributions (e.g., water content), topography, rheology or cohesion have been used to model landslide scaling (D'Ambrosio et al., 2003; Pelletier et al., 1997). Preexisting slope heterogeneity (e.g., variability in mechanical properties) was also proposed as the origin of power law distributions (Katz and Aharonov, 2006). Cellular automata based on a deterministic model (e.g., SCIDDICA) can simulate a debris flow process, although its applicability is dependent on the parameters involved in the real process to be simulated (D'Ambrosio et al., 2003). Another alternative model produces power scaling at large events on the basis of Mohr–Coulomb mechanics. The model, as a result of sediment cohesion, also captures the common rollover described in noncumulative frequency plots for small landslides (Jeandet et al., 2019).

5.4. Instabilities and hazards

Regional landslide hazard assessment, beyond any deterministic analysis of slope stability in a particular area, must address the long-term evolution of instability activity on a margin; this means characterising not only the magnitude-frequency but also the timing of the landslides. The probability of landslide-generated tsunamis depends on the number, size, location and frequency of large submarine landslides. Moreover, even small landslides are important for improved hazard analysis because their location (e.g., depth) is also a direct threat to infrastructure and may trigger local but destructive tsunamis.

The Palomares continental margin is intensively affected by mass movements, although the capacity of the process to mobilise sediment is limited compared with that of other passive margins. Large landslides have been inventoried, for example, along an area of approximately $562*10^3$ km^2 in the U.S. Atlantic margin. There, 106 events from 0.89 to 2400 km^2, affecting a total area of 15,275 km^2, and a total removed volume of 862 km^3 (ranging from 0.002 km^3 up to ~179 km^3) describe a scenario where large events affected a very large margin (Chaytor et al., 2009). Most likely, a better resolution of the DEM used for this inventory (100 m) would better define the sizes present along the margin, although this inventory outlines a margin 155 times larger, where the landslides are globally 16 times larger than those in Palomares and where the volume of sediments involved, for only 11.3 % of events described in Palomares, is 83 times larger.

Compared with the N Atlantic continental margins, the western Mediterranean contains only a few cases involving large areas and volumes of sediment (Urgeles and Camerlenghi, 2013). The magnitudes of instability in the study area are comparable to those in other Mediterranean areas where small and moderate events frequently occur (Casalbore et al., 2019; Casas et al., 2015; Casas et al., 2011; Casas et al., 2003; Katz et al., 2015; León et al., 2018; Martorelli et al., 2016). A comparable study was performed in the Gioia Basin (Tyrrhenian Sea), where 3350 km^2 of canyons, open slopes and highs were screened to find 428 reliable landslide scars affecting an area of more than 85 km^2 and a total volume of 1.4 km^3 (Casas et al., 2016). A rough comparison revealed 1 scar per 4 km^2 in the Palomares Basin and 1 scar every 8 km^2 in the Gioia Basin, where the area and volume are approximately ten times smaller; however, both cases can be defined as small to moderate events. No other detailed study has been conducted in the W Mediterranean, although a recent study in the neighbouring S Alboran Basin, located SW of the study area, described approximately sixty-seven instabilities on the seafloor or embedded in Quaternary sedimentary sequences, with average volumes of 0.41–4.8 km^3. Most instabilities are linked to structural highs or seamounts, although higher volumes of mobilised sediment occur on low slopes (d'Acremont et al., 2022). A similar situation has been described in the northern Alboran Basin, where instabilities are linked to highs and open slopes, affecting the contouritic sediments that build the continental slopes of the S Iberian margins (Alonso et al., 2016; Casas et al., 2011). Contourites are usually prone to failure, which is consistent with observations in the study area and in other areas around the Iberian Peninsula (Silva et al., 2020; Teixeira et al., 2023; Teixeira et al., 2020; Teixeira et al., 2019), although their role in slope instability in Alboran is yet to be revised (Yenes et al., 2021).

The timing of landslides is a generally outstanding question that has not yet been satisfactorily resolved. Timing is largely linked to triggers and preconditioning factors, including earthquakes, rapid sedimentation and sea level (Hampton et al., 1996; Talling et al., 2014). However, the role of these factors is sometimes poorly understood because, for example, not all large earthquakes (e.g., Mw 7) trigger large landslides (Völker et al., 2011; Sumner et al., 2013). Additionally, different margins respond differently to sea level; in high-latitude margins, large landslides correlate with rising sea levels and high stands, whereas in low-latitude margins, they seem to correlate with low stands. However, there is not a clear picture of those events with moderate or small sizes for which timing hypotheses are weakly tested. Real random ages and uncertainties in measuring ages may result in statistical results in the same frequency model (Urlaub et al., 2013). Uncertainties in landslide ages of ±3 kyr may result in a nearly random distribution of ages, even for nonrandom triggers (Pope et al., 2015).

There are significant uncertainties, poorly calibrated ages, in almost all submarine instabilities in the western Mediterranean Sea, including the Palomares margin. There, landslides were extensive and recurrent during the Plio-Quaternary. Recurrence seems to have increased during the last period of the Plio-Quaternary, although no available data allow a precise approach to determine the instability frequency in the area (Ercilla et al., 2022). Similar information is available in the neighbouring W Alboran Basin, where recently studied instabilities are estimated to be younger than 0.7–1.12 Ma because of their stratigraphic position (d'Acremont et al., 2022; Galindo-Zaldivar et al., 2018, among others). Therefore, collecting seafloor samples to date landslides accurately and reducing the large margin of error is one of the pending tasks of the marine hazard scientific community.

In summary, regional landslide hazard assessment is still a challenge regarding where landslides occur (i.e., size-frequency; ratio of small/large landslides; maximum size) and where they are expected to occur (e.g., Mueller et al., 2016). Although landslides become attractors for future landslides that tend to cluster, reliable models must be designed for analyses with respect to landslide susceptibility.

6. Conclusions

- Along more than 3620 km^2 of the Palomares continental slope, 936 scars were identified and characterised; this implies approximately 0.25 scars/km^2. The characteristic instability is defined for the area of 0.356 km^2, with a mean volume of 0.0108 km^3, which is comparable to findings in other Mediterranean areas where small to moderate events dominate. However, on the Palomares margin, recent instability has been especially common and intense.
- Mass movements affect 918.04 km^2 and involve 10.34 km^3 of eroded sediments from canyon walls, structural/volcanic highs and contouritic sediments deposited along the open slope; this represents an average of 2.8 million m^3 for each km^2.
- Null or scarce slight significant correlations between morphometric variables were found; this finding indicates that although smaller scars with a higher headwall gradient seem to dominate when the environment is steeper, a wide range of sizes may occur on any slope. There is no characteristic size for a particular slope gradient. Major mass movements are located in open slopes and structural highs, although a wide range of sizes can also occur at any observable depth.
- The cumulative size distribution (i.e., the probability function) is defined by a power-law function that describes events larger than 0.7 km^2 with an exponent of $\alpha = 1.269$. These results are consistent with those of other published inventories, including onshore cases, where power law behaviour is described for a limited range of large events.
- The scaling exponent α values range from 1.1 to 1.49 for the 3 defined data subsets (i.e., canyon walls, structural/volcanic highs and open slopes). These results are consistent with other reported scaling exponents despite their systematic variations. More work is needed to solve the uncertainty in determining exponents.
- Scaling exponents are useful for comparing inventories, i.e., the quantitative impact of sedimentary instabilities for different geologic frameworks, for comparing different resolution inventories and for developing new hazard probabilistic models considering large/small size ratios.
- The observed scale-invariant properties can be explained by different models, SOC vs. alternative models, each with important geomorphological implications in terms of landslide distribution and the long-term landslide history of any slope. To advance this goal, alternative working scenarios, such as submarine scenarios, contribute valuable and complementary observations to onshore inventories.

Supplementary data to this article can be found online at https://doi.org/10.1016/j.margeo.2024.107411.

CRediT authorship contribution statement

L. Retegui: Writing – original draft, Methodology, Investigation, Formal analysis, Conceptualization. **D. Casas:** Writing – original draft, Investigation, Funding acquisition, Conceptualization. **D. Casalbore:** Writing – original draft, Conceptualization. **M. Yenes:** Methodology, Investigation. **J. Nespereira:** Methodology, Investigation. **F. Estrada:** Writing – review & editing, Data curation. **A. Canari:** Writing – review & editing. **F.L. Chiocci:** Writing – review & editing, Validation. **J. Idárraga-García:** Writing – review & editing, Validation. **M. Teixeira:** Writing – review & editing, Validation. **J. Ramos:** Writing – review & editing. **N. López-Gonzalez:** Writing – review & editing.

Declaration of competing interest

The authors declare that they have no known competing financial interests or personal relationships that could have appeared to influence the work reported in this paper.

Data availability

Casas, D., & UTM-CSIC. (2018). FAUCES-2 Cruise, RV Sarmiento de Gamboa [Dataset]. UTM-CSIC. https://doi.org/10.20351/29SG20181004

Casas, David; Estrada, Ferran; López-González, Nieves; Retegui-Schiettekatte, Leire Anne; 2024; Submarine Mass Movements on the Palomares Continental Slope (W Mediterranean). Morphometric data inventory [Dataset], DIGITAL.CSIC; https://doi.org/10.20350/digitalCSIC/16560; http://hdl.handle.net/10261/368171

Acknowledgements

This research received support from the Spanish projects inGRAVITAS (PID2022-138258OB-I00), STRENGH (PID2019-104668RB-I00) and FAUCES (CTM2015-65461-C2-1-R). The authors from ICM-CSIC also thank the 'Severo Ochoa Centre of Excellence' for accreditation (CEX2019-000928-S). The authors thank the data provided by the General Spanish Secretary for Fisheries (SGP). We would like to thank the anonymous reviewers and Dr. M.A. Clare for their helpful comments, which greatly improved the article.

References

Alonso, B., Ercilla, G., Garcia, M., Vàzquez, J.T., Juan, C., Casas, D., Estrada, F., D'Acremont, E., Gorini, C., El Moumni, B., Farran, M., 2016. Quaternary mass-transport deposits on the North-Eastern Alboran Seamounts (SW Mediterranean Sea). Submarine mass movements and their consequences. In: 6th International Symposium, pp. 561–570. https://doi.org/10.1007/978-3-319-00972-8_50.

Alonso, B., Ercilla, G., Juan, C., López-González, N., Cacho, I., Francés, G., Palomino, D., Bárcenas, P., Yenes, M., Nespereira, J., Ausín, B., Mata, P., Casas, D., 2023. Contourite stratigraphic models linked to the light intermediate versus dense deep Mediterranean water flow regime variations (Alboran Sea, SW Mediterranean). Mar. Geol. 465. https://doi.org/10.1016/J.MARGEO.2023.107147.

Bak, P., Tang, C., Wiesenfeld, K., 1988. Self-organized criticality. Phys. Rev. 38, 364–374. https://doi.org/10.1103/physreva.38.364.

Casalbore, D., Bosman, A., Casas, D., Chiocci, F., Martorelli, E., Ridente, D., 2019. Morphological variability of submarine mass movements in the tectonically–Controlled calabro–Tyrrhenian continental margin (Southern Italy). Geosciences (Switzerland) 9. https://doi.org/10.3390/geosciences9010043.

Casas, D., Ercilla, G., Baraza, J., Alonso, B., Maldonado, A., 2003. Recent mass-movement processes on the Ebro continental slope (NW Mediterranean). Mar. Pet. Geol. 20, 445–457. https://doi.org/10.1016/S0264-8172(03)00078-3.

Casas, D., Ercilla, G., Yenes, M., Estrada, F., Alonso, B., García, M., Somoza, L., 2011. The Baraza Slide: Model and dynamics. Mar. Geophys. Res. 32, 245–256. https://doi.org/10.1007/s11001-011-9132-2.

Casas, D., Casalbore, D., Yenes, M., Urgeles, R., 2015. Submarine mass movements around the iberian Peninsula. The building of continental margins through hazardous processes. Bol. Geol. Min. 126, 257–278.

Casas, D., Chiocci, F., Casalbore, D., Ercilla, G., de Urbina, J.O., 2016. Magnitude-frequency distribution of submarine landslides in the Gioia Basin (southern Tyrrhenian Sea). Geo-Mar. Lett. 36, 405–414. https://doi.org/10.1007/s00367-016-0458-2.

Casas, D., Ercilla, G., Alonso, B., Yenes, M., Casalbore, D., Nespereira, J., Estrada, F., Chiocci, F., Idarraga-García, J., Teixeira, M., Ceramicola, S., Fauces, T., 2019. Submarine mass movements affecting the submarine Almanzora-Alías-Garrucha canyon (SW Mediterranean). In: 34th IAS Meeting of Sedimentology "Sedimentology to Face Societal Challenges on Risk, Resources and Record of the Past." Rome.

Chaytor, J.D., ten Brink, U.S., Solow, A.R., Andrews, B.D., 2009. Size distribution of submarine landslides along the U.S. Atlantic Margin. Mar. Geol. 264, 16–27. https://doi.org/10.1016/J.MARGEO.2008.08.007.

Clare, M.A., Vardy, M.E., et al., 2017. Direct monitoring of active geohazards: emerging geophysical tools for deep-water assessments. Near Surface Geophys. 15, 427–444.

Clare, M., Chaytor, J., Dabson, O., Gamboa, D., Georgiopoulou, A., Eady, H., Hunt, J., Jackson, C., Katz, O., Krastel, S., León, R., 2019. A consistent global approach for the morphometric characterization of subaqueous landslides. Geol. Soc. Lond. Spec. Publ. 477 (1), 455–477.

Clauset, A., Rohilla Shalizi, C., Newman, J.M.E., 2009. Power-Law Distributions in Empirical Data *. Soc. Ind. Appl. Math. 51, 661–703. https://doi.org/10.1137/070710111.

Coppier, G., Griveaud, P., de Larouziere, F.-D., Montenat, C., Ott d'Estevou, P., 1989. Example of Neogene tectonic indentation in the Eastern Betic Cordilleras: the Arc of Aguilas (Southeastern Spain). Geodin. Acta 3, 37–51. https://doi.org/10.1080/09853111.1989.11105173.

d'Acremont, E., Lafuerza, S., Rabaute, A., Lafosse, M., Jollivet Castelot, M., Gorini, C., Alonso, B., Ercilla, G., Vazquez, J.T., Vandorpe, T., Juan, C., Migeon, S., Ceramicola, S., Lopez-Gonzalez, N., Rodriguez, M., El Moumni, B., Benmarha, O., Ammar, A., 2022. Distribution and origin of submarine landslides in the active margin of the southern Alboran Sea (Western Mediterranean Sea). Mar. Geol. 445, 106739. https://doi.org/10.1016/J.MARGEO.2022.106739.

D'Ambrosio, D., Di Gregorio, S., Iovine, G., 2003. Simulating debris flows through a hexagonal cellular automata model: SCIDDICA S_{3-hex}. Nat. Hazards Earth Syst. Sci. 3, 545–559. https://doi.org/10.5194/NHESS-3-545-2003.

Densmore, A.L., Ellis, M.A., Anderson, R.S., 1998. Landsliding and the evolution of normal-fault-bounded mountains. J. Geophys. Res. 103, 203–218. https://doi.org/10.1029/98JB00510.

Ercilla, G., Juan, C., Hernández-Molina, F.J.J., Bruno, M., Estrada, F., Alonso, B., Casas, D., Farran, M. lí, Llave, E., García, M., Vázquez, J.T.T., D'Acremont, E., Gorini, C., Palomino, D., Valencia, J., El Moumni, B., Ammar, A., 2016. Significance of bottom currents in deep-sea morphodynamics: an example from the Alboran Sea. Mar. Geol. 378, 157–170. https://doi.org/10.1016/j.margeo.2015.09.007.

Ercilla, G., Casas, D., Alonso, B., Casalbore, D., Galindo-Zaldívar, J., García-Gil, S., Martorelli, E., Vázquez, J.-T., Azpiroz-Zabala, M., DoCouto, D., Estrada, F., Fernández-Puga, M.C., González-Castillo, L., González-Vida, J.M., Idárraga-García, J., Juan, C., Macías, J., Madarieta-Txurruka, A., Nespereira, J., Palomino, D., Sánchez-Guillamón, O., Tendero-Salmerón, V., Teixeira, M., Valencia, J., Yenes, M., 2021. Offshore geological hazards: charting the course of progress and future directions. Oceans 2 (2), 393–428. https://doi.org/10.3390/oceans2020023.

Ercilla, G., Galindo-Zaldívar, J., Estrada, F., Valencia, J., Juan, C., Casas, D., Alonso, B., Comas, M.C., Tendero-Salmerón, V., Casalbore, D., Azpiroz-Zabala, M., Bárcenas, P., Ceramicola, S., Chiocci, F.L., Idárraga-García, J., López-González, N., Mata, P., Palomino, D., Rodríguez-García, J.A., Teixeira, M., Nespereira, J., Vázquez, J.T., Yenes, M., 2022. Understanding the complex geomorphology of a deep sea area affected by continental tectonic indentation: the case of the Gulf of Vera (Western Mediterranean). Geomorphology 402. https://doi.org/10.1016/J.GEOMORPH.2022.108126.

Estrada, F., Ercilla, G., Gorini, C., Alonso, B., Vazquez, J.T., García-Castellanos, D., Juan, C., Maldonado, A., Ammar, A., Elabbassi, M., 2011. Impact of pulsed Atlantic water inflow into the Alboran Basin at the time of the Zanclean flooding. Geo-Mar. Lett. 31, 361–376. https://doi.org/10.1007/s00367-011-0249-8.

Evesque, P., 1991. Analysis of the statistics of sandpile avalanches using soil-mechanics results and concepts. Phys. Rev. A (Coll Park) 43, 2720. https://doi.org/10.1103/PhysRevA.43.2720.

Feder, J., 1988. Fractals. https://doi.org/10.1007/978-1-4899-2124-6.

Fuyii, Y., 1969. Frequency distribution of the magnitude of the landslides caused by heavy rainfall. J. Seismol. Soc. Jpn. 22, 244–247.

Galindo-Zaldivar, J., Ercilla, G., Estrada, F., Catalán, M., D'Acremont, E., Azzouz, O., Casas, D., Chourak, M., Vazquez, J.T., Chalouan, A., Sanz de Galdeano, C., Benmakhlouf, M., Gorini, C., Alonso, B., Palomino, D., Rengel, J.A., Gil, A.J., 2018. Imaging the growth of recent Faults: the Case of 2016–2017 Seismic Sequence Sea Bottom Deformation in the Alboran Sea (Western Mediterranean). Tectonics 37, 2513–2530. https://doi.org/10.1029/2017TC004941.

Galli, M., Ardizzone, F., Cardinali, M., Guzzetti, F., Reichenbach, P., 2007. Comparing landslide inventory maps. https://doi.org/10.1016/j.geomorph.2006.09.023.

Giaconia, F., Booth-Rea, G., Martínez-Martínez, J.M., Azañón, J.M., Pérez-Peña, J.V., 2012. Geomorphic analysis of the Sierra Cabrera, an active pop-up in the constrictional domain of conjugate strike-slip faults: the Palomares and Polopos fault zones (eastern Betics, SE Spain). Tectonophysics 580, 27–42. https://doi.org/10.1016/J.TECTO.2012.08.028.

Gómez de la Peña, L., Gràcia, E., Muñoz, A., Acosta, J., Gómez-Ballesteros, M., Ranero, C., Uchupi, E., 2016. Geomorphology and Neogene tectonic evolution of the Palomares continental margin (Western Mediterranean). Tectonophysics 689, 25–39. https://doi.org/10.1016/J.TECTO.2016.03.009.

Guthrie, R.H., Evans, S.G., 2004. Magnitude and frequency of landslides triggered by a storm event, Loughborough Inlet, British Columbia. Nat. Hazards Earth Syst. Sci. 4, 475–483. https://doi.org/10.5194/NHESS-4-475-2004.

Guzzetti, F., Malamud, B.D., Turcotte, D.L., Reichenbach, P., 2002. Power-law correlations of landslide areas in Central Italy. Earth Planet. Sci. Lett. 195, 169–183. https://doi.org/10.1016/S0012-821X(01)00589-1.

Guzzetti, F., Reichenbach, P., Cardinali, M., Galli, M., Ardizzone, F., 2005. Probabilistic landslide hazard assessment at the basin scale. Geomorphology 72, 272–299. https://doi.org/10.1016/J.GEOMORPH.2005.06.002.

Guzzetti, F., Ardizzone, F., Cardinali, M., Rossi, M., Valigi, D., 2009. Landslide volumes and landslide mobilization rates in Umbria, Central Italy. Earth Planet. Sci. Lett. 279, 222–229. https://doi.org/10.1016/J.EPSL.2009.01.005.

Guzzetti, F., Mondini, A.C., Cardinali, M., Fiorucci, F., Santangelo, M., Chang, K.-T., 2012. Landslide inventory maps: New tools for an old problem. https://doi.org/10.1016/j.earscirev.2012.02.001.

Haflidason, H., Lien, R., Sejrup, H.P., Forsberg, C.F., Bryn, P., 2005. The dating and morphometry of the Storegga Slide. Mar. Pet. Geol. 22, 123–136. https://doi.org/10.1016/J.MARPETGEO.2004.10.008.

Hampton, M.A., Lee, H.J., Locat, J., 1996. Submarine landslides. Rev. Geophys. 34, 33–59. https://doi.org/10.1029/95RG03287.

Harbitz, C.B., Løvholt, F., Bungum, H., 2014. Submarine landslide tsunamis: how extreme and how likely? Nat. Hazards 72, 1341–1374. https://doi.org/10.1007/s11069-013-0681-3.

Harp, E.L., Jibson, R.W., 1995. Inventory of Landslides Triggered by the 1994 Northridge, California earthquake. Open-File Report. https://doi.org/10.3133/OFR95213.

Hergarten, S., 2002. Self-Organized Criticality in Earth Systems. Self-Organized Criticality in Earth Systems. https://doi.org/10.1007/978-3-662-04390-5.

Hovius, N., Stark, C.P., Allen, P.A., 1997. Sediment flux from a mountain belt derived by landslide mapping. Geology 25, 231–234.

Hu, G., Yan, T., Liu, Z., Vanneste, M., Dong, L., 2009. Size distribution of submarine landslides along the middle continental slope of the East China Sea. J. Ocean Univ. China 8, 322–326.

Hühnerbach, V., Masson, D.G., 2004. Landslides in the North Atlantic and its adjacent seas: an analysis of their morphology, setting and behaviour. Mar. Geol. 213, 343–362.

Hungr, O., Leroueil, S., Picarelli, L., 2014. The Varnes classification of landslide types, an update. Landslides 11, 167–194. https://doi.org/10.1007/S10346-013-0436-Y/FIGURES/23.

Jeandet, L., Steer, P., Lague, D., Davy, P., 2019. Coulomb Mechanics and Relief Constraints Explain Landslide size distribution. Geophys. Res. Lett. 46, 4258–4266. https://doi.org/10.1029/2019GL082351.

Juan, C., Ercilla, G., Javier Hernández-Molina, F., Estrada, F., Alonso, B., Casas, D., García, M., Farran, M., Llave, E., Palomino, D., Vázquez, J.T., Medialdea, T., Gorini, C., D'Acremont, E., El Moumni, B., Ammar, A., 2016. Seismic evidence of current-controlled sedimentation in the Alboran Sea during the Pliocene and Quaternary: Palaeoceanographic implications. Mar. Geol. 378, 292–311. https://doi.org/10.1016/J.MARGEO.2016.01.006.

Juan, C., Ercilla, G., Estrada, F., Alonso, B., Casas, D., Vázquez, J.T., d'Acremont, E., Medialdea, T., Hernández-Molina, F.J., Gorini, C., El Moumni, B., Valencia, J., 2020. Multiple factors controlling the deep marine sedimentation of the Alboran Sea (SW Mediterranean) after the Zanclean Atlantic Mega-flood. Mar. Geol. 423. https://doi.org/10.1016/J.MARGEO.2020.106138.

Katz, O., Aharonov, E., 2006. Landslides in vibrating sand-box: what controls types of slope-failure and frequency magnitude relations? Earth Planet. Sci. Lett. 247, 280–294.

Katz, O., Reuven, E., Aharonov, E., 2015. Submarine landslides and fault scarps along the eastern Mediterranean Israeli continental-slope. Mar. Geol. 369, 100–115.

Klar, A., Aharonov, E., Kalderon-Asael, B., Katz, O., 2011. Analytical and observational relations between landslide volume and surface area. Case Rep. Med. 116, 2001. https://doi.org/10.1029/2009JF001604.

Kvalstad, T.J., Andresen, L., Forsberg, C.F., Berg, K., Bryn, P., Wangen, M., 2005. The Storegga Slide: evaluation of triggering sources and slide mechanics. Mar. Pet. Geol. 22, 245–325. https://doi.org/10.1016/j.marpetgeo.2004.10.019.

León, R., García-Davalillo, J.C., Casas, D., Giménez-Moreno, C.J., 2018. Submarine landslide catalogue onshore/offshore harmonization: Spain as a case study. In: 8th International Symposium on Submarine Mass Movements and their Consequences, ISSMMTC 2018, pp. 497–510. https://doi.org/10.1144/SP477.38.

León, R., Urgeles, R., Pérez-López, R., Payo, E., Izquierdo, A.V., Giménez-Moreno, C.J., Casas, D., 2020. Geological and tectonic controls on morphometrics of submarine landslides of the spanish margins. Geol. Soc. Spec. Publ. 500, 495–513. https://doi.org/10.1144/SP500-2019-153.

Locat, J., Lee, H.J., 2002. Submarine landslides: advances and challenges. Can. Geotech. J. 39, 193–212. https://doi.org/10.1139/t01-089.

Malamud, Bruce D., Turcotte, D.L., Guzzetti, F., Reichenbach, P., 2004. Landslide inventories and their statistical properties. Earth Surf. Process. Landf. 29, 687–711. https://doi.org/10.1002/ESP.1064.

Martorelli, E., Bosman, A., Casalbore, D., Falcini, F., 2016. Interaction of down-slope and along-slope processes off Capo Vaticano (southern Tyrrhenian Sea, Italy), with particular reference to contourite-related landslides. Mar. Geol. 378, 43–55. https://doi.org/10.1016/J.MARGEO.2016.01.005.

Micallef, A., Berndt, C., Masson, D.G., Stow, D.A.V., 2007. Fractal statistics of the Storegga Slide. In: Lykousis, V., Sakellariou, D., Locat, J. (Eds.), Submarine Mass Movements and Their Consequences. Advances in Natural and Technological Hazards Research, vol. 27. Springer, Dordrecht. https://doi.org/10.1007/978-1-4020-6512-5_1.

Micallef, A., Berndt, C., Masson, D.G., Stow, D.A., 2008. Scale invariant characteristics of the Storegga Slide and implications for large-scale submarine mass movements. Mar. Geol. 247 (1–2), 46–60.

Moscardelli, L., Wood, L., 2016. Morphometry of mass-transport deposits as a predictive tool. GSA Bull. 128, 47–80. https://doi.org/10.1130/B31221.1.

Mueller, C., Mountjoy, J., Power, W., Lane, E., Wang, X., 2016. Towards a spatial probabilistic submarine landslide hazard model for submarine canyons. In: Submarine Mass Movements and their Consequences: 7th International Symposium. Springer International Publishing, pp. 589–597.

Mulder, T., Cochonat, P., 1996. Classification of offshore mass movements. J. Sediment. Res. 66, 43–57. https://doi.org/10.1306/D42682AC-2B26-11D7-8648000102C1865D.

Nagel, S.R., 1992. Instabilities in a sandpile. Rev. Mod. Phys. 64, 321. https://doi.org/10.1103/RevModPhys.64.321.

Nardin, T.R., Hein, F.J., Gorsline, D.S., Edwards, B.D., 1979. A review of mass movement processes, sediment and acoustic characteristics, and contrasts in slope and base-of-slope systems versus Canyon-Fan-Basin floor systems. Geol. Continental Slopes 61–73. https://doi.org/10.2110/PEC.79.27.0061.

Pelletier, J.D., Malamud, B.D., Blodgett, T., Turcotte, D.L., 1997. Scale-invariance of soil moisture variability and its implications for the frequency-size distribution of landslides. Eng. Geol. 48, 2555268.

Pope, E.L., Talling, P.J., Urlaub, M., Hunt, J.E., Clare, M.A., Challenor, P., 2015. Are large submarine landslides temporally random or do uncertainties in available age constraints make it impossible to tell? Mar. Geol. 369, 19–33. https://doi.org/10.1016/J.MARGEO.2015.07.002.

Puga-Bernabéu, Á., López-Cabrera, J., Webster, J.M., Beaman, R.J., 2022. Submarine landslide morphometrics and slope failure dynamics along a mixed carbonate-siliciclastic margin, North-Eastern Australia. Geomorphology 403, 108179. https://doi.org/10.1016/J.GEOMORPH.2022.108179.

Rafiei, A., Rahman, M.S., Gabr, M.A., 2019. Coupled analysis for response and instability of sloping seabed under wave action. Appl. Ocean Res. 88, 99–110. https://doi.org/10.1016/J.APOR.2019.04.017.

Shanmugam, G., 2019. Slides, slumps, debris flows, turbidity currents, hyperpycnal flows, and bottom currents. In: Encyclopedia of Ocean Sciences. https://doi.org/10.1016/B978-0-12-409548-9.10884-X.

Silva, P.F., Roque, C., Drago, T., Belén, A., Henry, B., Gemma, E., Lopes, A., López-González, N., Casas, D., Naughton, F., Vázquez, J.T., 2020. Multidisciplinary characterization of Quaternary mass movement deposits in the Portimão Bank (Gulf of Cadiz, SW Iberia). Mar. Geol. 420. https://doi.org/10.1016/j.margeo.2019.106086.

Stark, C.P., Guzzetti, F., 2009. Landslide rupture and the probability distribution of mobilized debris volumes. Case Rep. Med. 114. https://doi.org/10.1029/2008JF001008.

Stark, C.P., Hovius, N., 2001. The characterization of landslide size distributions. Geophys. Res. Lett. 28, 1091–1094. https://doi.org/10.1029/2000GL008527.

Sugai, T., Ohmori, H., Hirano, M., 1995. Rock control on magnitude-frequency distribution of landslide. Int. J. Rock Mech. Min. Sci. Geomech. Abstr. 3, 116A.

Sultan, N., Cochonat, P., Foucher, J.-P., Mienert, J., 2004. Effect of gas hydrates melting on seafloor slope instability. Mar. Geol. 213, 379–401.

Sumner, E., Siti, M.I., McNeill, L., Talling, P.J., Henstock, T.J., Wynn, R.B., Djajadihardja, Y., Permana, H., 2013. Can turbidites be used to reconstruct a palaeoearthquake record for the central Sumatran margin? Geology 41 (7), 763–766. https://doi.org/10.1130/G34298.1.

Talling, P.J., Clare, M.L., Urlaub, M., Pope, E., Hunt, J.E., Watt, S.F., 2014. Large submarine landslides on continental slopes: geohazards, methane release, and climate change. Oceanography 27, 32–45.

Tanyaş, H., van Westen, C.J., Allstadt, K.E., Jibson, R.W., 2019. Factors controlling landslide frequency–area distributions. Earth Surf. Process. Landf. 44, 900–917. https://doi.org/10.1002/ESP.4543.

Tebbens, S.F., 2020. Landslide Scaling: a Review. Earth Space Sci. https://doi.org/10.1029/2019EA000662.

Teixeira, M., Terrinha, P., Roque, C., Rosa, M., Ercilla, G., Casas, D., 2019. Interaction of alongslope and downslope processes in the Alentejo margin (SW Iberia) – Implications on slope stability. Mar. Geol. 410, 88–108. https://doi.org/10.1016/j.margeo.2018.12.011.

Teixeira, M., Terrinha, P., Roque, C., Voelker, A.H.L., Silva, P., Salgueiro, E., Abrantes, F., Naughton, F., Mena, A., Ercilla, G., Casas, D., 2020. The late Pleistocene-Holocene sedimentary evolution of the Sines Contourite Drift (SW Portuguese margin): a multiproxy approach. Sediment. Geol. 407. https://doi.org/10.1016/J.SEDGEO.2020.105737.

Teixeira, M., Roque, C., Omira, R., Marques, F., Gamboa, D., Terrinha, P., Ercilla, G., Yenes, M., Mena, A., Casas, D., 2023. Submarine landslide hazard in the Sines Contourite Drift, SW Iberia: slope instability analysis under static and transient conditions. Nat. Hazards. https://doi.org/10.1007/s11069-023-06340-z.

ten Brink, U.S., Geist, E.L., Andrews, B.D., 2006. Size distribution of submarine landslides and its implication to tsunami hazard in Puerto Rico. Geophys. Res. Lett. 33. https://doi.org/10.1029/2006GL026125.

Turcotte, D.L., 1999. Self-organized criticality. Rep. Prog. Phys. 62, 1377. https://doi.org/10.1088/0034-4885/62/10/201.

Urgeles, R., Camerlenghi, A., 2013. Submarine landslides of the Mediterranean Sea: Trigger mechanisms, dynamics, and frequency-magnitude distribution. Case Rep. Med. 118, 2600–2618. https://doi.org/10.1002/2013JF002720.

Urgeles, R., Gamboa, D., Leon, R., Lovholt, F., Vanneste, M., Cattaneo, A., Cattaneo, A.C., 2023. The EuroMediterranean submarine landslide database: towards offshore geohazard quantitative assessement from submarine landslides and derived Tsunamis. In: EGU General Assembly. Viena.

Urlaub, M., Talling, P.J., Masson, D.G., 2013. Timing and frequency of large submarine landslides: Implications for understanding triggers and future geohazard. Quat. Sci. Rev. 72, 63–82. https://doi.org/10.1016/J.QUASCIREV.2013.04.020.

Van Den Eeckhaut, M., Poesen, J., Govers, G., Verstraeten, G., Demoulin, A., 2007. Characteristics of the size distribution of recent and historical landslides in a

populated hilly region. Earth Planet. Sci. Lett. 256, 588–603. https://doi.org/10.1016/J.EPSL.2007.01.040.
Völker, D., Scholz, F., Geersen, J., 2011. Analysis of submarine landsliding in the rupture area of the 27 February 2010 Maule earthquake, Central Chile. Mar. Geol. 288, 79–89.
Wang, L., Zhang, J., Jeng, D.S., Zhang, Q., Chen, T., 2023. Experimental study on the dynamic response of a silty seabed under waves. Ocean Eng. 269, 113554. https://doi.org/10.1016/J.OCEANENG.2022.113554.
Williams, J.G., Rosser, N.J., Hardy, R.J., Brain, M.J., Afana, A.A., 2018. Optimising 4-D surface change detection: an approach for capturing rockfall magnitude-frequency. Earth Surf. Dyn. 6, 101–119. https://doi.org/10.5194/ESURF-6-101-2018.
Yenes, M., Casas, D., Nespereira, J., López-González, N., Casalbore, D., Monterrubio, S., Alonso, B., Ercilla, G., Juan, C., Bárcenas, P., Palomino, D., Mata, P., Martínez-Díaz, P., Pérez, N., Vázquez, J.T., Estrada, F., Azpiroz-Zabala, M., Teixeira, M., 2021. The Guadiaro-Baños contourite drifts (SW Mediterranean). A geotechnical approach to stability analysis. Mar. Geol. 437. https://doi.org/10.1016/j.margeo.2021.106505.